Extreme Mechanics Letters 32 (2019) 100566

Contents lists available at ScienceDirect

Extreme Mechanics Letters

journal homepage: www.elsevier.com/locate/eml

A contraction–reaction–diffusion model: Integrating biomechanics and biochemistry in cell migration

Bahador Marzban [b,1], Jiming Kang [a,b,1], Ningwei Li [c], Yubing Sun [c], Hongyan Yuan [a,b,*]

[a] Department of Mechanics and Aerospace Engineering, Southern University of Science and Technology, Shenzhen, Guangdong 518055, China
[b] Department of Mechanical, Industrial & Systems Engineering, University of Rhode Island, Kingston, RI 02881, USA
[c] Department of Mechanical and Industrial Engineering, University of Massachusetts, Amherst, MA 01003, USA

ARTICLE INFO

Article history:
Received 12 September 2019
Received in revised form 15 September 2019
Accepted 15 September 2019
Available online 18 September 2019

Keywords:
Mechanobiology
Cell migration
Cytoskeletal contraction
Reaction–diffusion
Durotaxis

ABSTRACT

Cell migration is a fundamental biological process involved in many physiological and pathological processes. To understand how cell migration works at the whole cell level, biomechanical and biochemical models have been developed but were mainly independent of each other. In this work, we developed a mechanobiochemical model for cell migration at the whole-cell scale. In the model, mechanics of cytoskeleton contraction generates distributed forces for the cell to sense the mechanical properties of itself and its microenvironment. The mechanosensing is coupled with the signaling network of reaction–diffusion of biomolecules in the cell. The computational results show that the model can simulate cell polarization (head-to-tail formation) and shape-dependent localization of the protrusion signal. Furthermore, this dynamic model of cell migration can recapitulate durotaxis *in silicon* and simulate cellular morphogenesis.

Published by Elsevier Ltd.

1. Introduction

Cell migration, an intriguing phenomenon involved in tissue formation and cancer metastasis, has long been the subject of intensive investigation in the fields of biophysics and cell biology [1]. The machineries that drive migration, and the signaling networks that control the migration machineries have been studied intensively [2]. In vitro 2D cell migration experiments revealed that cells of different types, such as fibroblasts, keratocytes, and neurons, exhibit different migration/spreading behaviors. On the other hand, different types of cells share some fundamental characteristics. In general, single cell migration can be described as a coordinated and integrated process of different modules (Fig. 1): cell polarization (i.e., front-and-rear formation), protrusion of lamellipodia/filopodia/lobopodia, invadopodia formation and proteolysis of surrounding ECM, formation of new adhesions in the front, releasing of aging adhesions at the rear, and cytoskeleton/membrane skeleton contraction to move the rear forward [2,3]. Intensive research has been carried out to mathematical modeling of cell migration at different length scales from subcellular and cellular [4–6] to multicellular and tissue [7–11] levels. The present work is focused on the mathematical modeling of spatiotemporal integration of biomechanical and biochemical events involved in cell migration at the whole cell level.

Inspired by Turing's reaction–diffusion model of diffusive biochemical molecules, mathematical models were developed to study cell polarization [5] and cellular morphogenesis [12,13]. Particularly, the reaction and diffusion of intracellular signaling molecules have been interpreted as to form networks [14]. Cells with this internal network system are able to spontaneously polarize and to carry out directed movement when biased by external signal gradients (i.e., chemotaxis).

In recent years, it has been shown that cell migration can also be guided by a variety of mechanical cues of the microenvironment, such as substrate rigidity (i.e., durotaxis [15]), matrix topology (i.e., contact guidance [16]), shear flow (i.e., mechanotaxis [17]). It has been understood that mechanical cues are sensed by living cells through various mechanotransduction pathways [18–22], which refers to the conversion of mechanical force applied on the cell, either extracellularly or intracellularly (i.e., by active cell contraction), into biochemical signals. For example, integrin-based focal adhesions have been intensively studied in last decades for its new role of mechanosensing. The forces and deformations experienced in the focal adhesion were shown to not only reinforce focal adhesion formation but also elicit downstream signals to regulate other cellular processes such as membrane protrusion [23]. In addition, stresses in cytoskeleton and cell–cell adhesions were found to play a regulatory role in the

* Corresponding author at: Department of Mechanics and Aerospace Engineering, Southern University of Science and Technology, Shenzhen, Guangdong 518055, China.
E-mail address: yuanhy3@sustech.edu.cn (H. Yuan).

[1] B. Marzban and J. Kang contributed equally to this work.

https://doi.org/10.1016/j.eml.2019.100566
2352-4316/Published by Elsevier Ltd.

cytoskeleton organization and cell–cell adhesion formation [24, 25].

Biochemical models based on reaction–diffusion equations lack the consideration of mechanotransduction thus cannot capture mechanosensing in cell migration. Biomechanics models lack consideration of biochemical signaling and thus fail to account for biochemical processes. A thorough understanding of cell migration will require the elucidation of how the mechanical and biochemical events are spatiotemporally integrated at the cellular scale. It is possible that the stress-mediated downstream biochemical signals are wired to the same internal signaling networks for chemotaxis. In this work, we developed a contraction–reaction–diffusion model for cell migration by integrating the mechanical force generation and reaction–diffusion of biochemical molecules at the whole-cell scale. Our overarching hypothesis is the following: the biomechanical and biochemical signals form mechanobiochemical feedback loops [26, 27]. Through the mechanobiochemical feedback loop, cell migration can be regulated by a variety of mechanical cues, such as geometric constraints [28] and substrate rigidity gradient [29].

2. Methods

The present computational model is concerned with cells spreading and migrating on the surface of the substrate. Cells are modeled as a two-dimensional (2D) continuum, which reflects the flatness of the lamellipodia for cells cultured on 2D flat substrates. As illustrated in Fig. 1C, four physical domains are defined for the cell: cytoskeleton domain Ω_{CSK}, cytosol domain Ω_{Cyto}, membrane domain Ω_{Mem}, and substrate domain Ω_{Sub}. In the cell membrane domain Ω_{Mem}, reaction–diffusion equation of protrusion signaling molecules (membrane-bound) are formulated. In the cytosol domain Ω_{Cyto}, reaction–diffusion equation of retraction-related molecules are formulated. In the cytoskeleton domain Ω_{CSK}, elasticity theory is used and equilibrium equations concerning the mechanical stresses in cytoskeleton are formulated. Because 2D model of the cell is adopted, the physical domains Ω_{CSK}, Ω_{Cyto}, Ω_{Mem}, and Ω_{Sub} can be described by the same mathematical domain Ω. The single-cell model is composed of several modules: cytoskeleton mechanics, reaction–diffusion of molecules, protrusion and retraction of cell body, cytoskeleton asymmetry, and cell–substrate interaction, which will be described below.

2.1. Cytoskeleton mechanics

A rather simple mechanics model of cytoskeleton is adopted here. Because the migration of biological cells in their solid or fluid microenvironment is at the low Reynolds number, the inertia force can be neglected. At each time instant, the cell can be considered in a quasi-static equilibrium. The equilibrium equation of the cytoskeleton in the domain Ω_{CSK} are written by using Cartesian tensor notation (summation over repeated indices is adopted hereinafter) as

$$h_c \sigma_{ij,j} - T_i = 0 \tag{1}$$

where σ_{ij} is the Cauchy stress tensor of the cytoskeleton (i and j takes values of 1 and 2 in 2D), h_c is the thickness of the cell, which is assumed to be uniform throughout the cell. Denoting A_c the area of the cell, the volume of the cell is calculated as

$$V_c = A_c h_c \tag{2}$$

The cell volume is assumed to be conserved in the present study, so h_c varies with time when the cell area changes. Here T_i is the traction stress exerted on the substrate by the cell. At the cell edge (denoted by Γ) where there is no cell–cell adhesion, the stress-free boundary condition holds: $\sigma_{ij} n_j = 0$, where n_j is the normal direction at the cell edge. In the present model, the cytoskeleton is composed of passive and active networks. For the sake of simplicity, a simple elastic constitutive relation is adopted,

$$\sigma_{ij} = 2G e_{ij} + K \varepsilon_{kk} \delta_{ij} + \Sigma_{ij} \tag{3}$$

where $\varepsilon_{ij} = \frac{1}{2}\left(u_{i,j} + u_{j,i}\right)$ is the strain tensor, u_i is the displacement, $e_{ij} = \varepsilon_{ij} - \varepsilon_{kk}/3$ is the deviatoric strain tensor, G and K are shear and bulk modulus of the passive network, Σ_{ij} is the active isometric tensile stress (ITS) tensor from the active part of the cytoskeleton, which will be defined later in Eq. (6). Use of the small-strain Hooke's law in Eq. (3) for the large deformation that occurs during cell motility deserves some explanations here. In this model, when solving the elasticity problem for a migrating cell, at each time instant we treat the current configuration as the stress-free state, and displacement u_i and strain ε_{ij} are measured from the current stress–stress configuration, rather than the reference state at the beginning of the simulation. This is a simplistic treatment based on the assumption that the time scale of cytoskeletal remodeling is shorter than that of the cell movement. The traction stress is assumed to be linearly proportional to the "instantaneous" displacement u_i of the cell

$$T_i = k_{cs} u_i \tag{4}$$

where k_{cs} is the spring constant of the cell–substrate linkage that will be defined later in Eq. (18). There have been more comprehensive finite-strain active viscoelastic models developed for living cells [30]. In this study, the simple mechanics model is adopted to facilitate the understanding of the integration of mechanics and biochemistry of the cell.

To account for the anisotropic fiber formation, a previously defined mathematical model for myofibril orientation in cardiomyocytes is used [28]. A second-order tensor S_{ij}, referred to as the stress-fiber structure tensor, is defined and its time evolution is described by

$$\frac{dS_{ij}}{dt} = K_{on}^S \frac{1}{\sigma_t + \sigma_m} \sigma_{ij} H(\sigma_t) - K_{off}^S S_{ij} \tag{5}$$

where K_{on}^S and K_{off}^S are the stress fiber activation and deactivation rates, respectively. Here, σ_m is a model parameter, $\sigma_t = \sigma_{kk}/2$ is the cytoskeletal tension, $H()$ denotes Heaviside function and is defined as: $H(x) = 1$ when $x > 0$ and $H(x) = 0$ when $x \leq 0$. Denoting the maximal eigenvalue and the corresponding eigenvector of S_{ij} by λ_1 and m_i^1, respectively, the ITS tensor Σ_{ij} is defined as

$$\Sigma_{ij} = (\sigma_{c0} + \sigma_{c1}\zeta)\,\delta_{ij} + \sigma_{cf} \lambda_1 m_i^1 m_j^1 \tag{6}$$

where σ_{c0}, σ_{c1}, and σ_{cf} denotes the baseline, retraction signal-associated, and stress fiber-associated contractility, ζ is the concentration of retraction signal that will be introduced below (It has been shown that there exists a time delay between the contraction signals and actomyosin contraction [31], here we have neglected this time delay in the model). The dyadic product of unit vector m_i^1 produces the tensor $m_i^1 m_j^1$, which has its only non-zero-principle-value principle direction along m_i^1. This anisotropic cytoskeleton model has been used to explain the pattern formation of myofibrils in single cardiomyocytes [28].

2.2. Reaction–diffusion of protrusion and retraction signals

In this work, we adopt a similar modeling approach as Satulovsky et al. [12] where a few phenomenological variables are used to represent the lumped effect of many different proteins involved in cell migration. Previous studies indicated that the

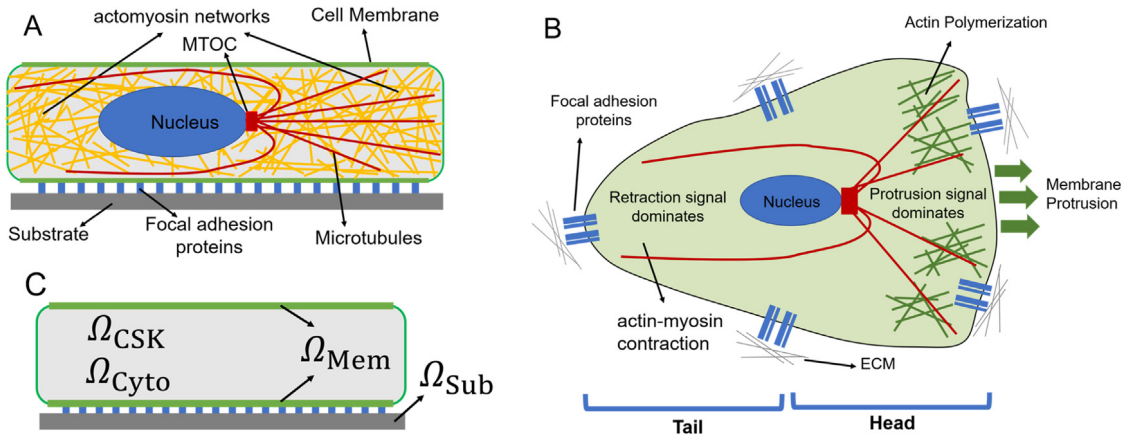

Fig. 1. Schematic illustrations of subcellular structures involved in the cell model. (A) Side view: macromolecular entities involved in cell migration. (B) Top view: head-to-tail formation in a polarized cell. (C) The physical domains involved in the continuum model of the cell. Note that the 2D mathematical domain is the top view shown in (B), not the cross-section of the cell in (A) and (C).

active forms of protrusion and retraction signals are membrane-bound proteins [13,32]. Two phenomenological variables ξ and ζ are defined in the physical domain of the membrane Ω_{Mem} to account for the area concentration of active form of protrusion (e.g., Rac, Cdc42) and retraction (e.g., ROCK) signals, respectively [12]. Here variables ξ and ζ are normalized by their saturation values respectively thus are in units of μm^{-2} and with the maximal value of 1 μm^{-2}. Their time evolution equations are defined as

$$\frac{D\xi}{\partial t} = D_\xi \Delta\xi + \left[\frac{K_0^\xi}{1+(\zeta/\zeta_0)^{n_1}} + K_T^\xi\left(\frac{T^{n_2}}{T^{n_2}+T_0^{n_2}}\right)\rho + K_M^\xi f_M \xi\right] \times (h_c\xi_i) - K_{\text{off}}^\xi \xi + \sqrt{R_\xi}\,G(t) \tag{7}$$

$$\frac{D\zeta}{\partial t} = D_\zeta \Delta\zeta + \left[\frac{K_0^\zeta}{1+(\xi/\xi_0)^{n_3}}\right](h_c\zeta_i) - K_{\text{off}}^\zeta \zeta + \sqrt{R_\zeta}\,G(t) \tag{8}$$

where $\frac{D}{\partial t}$ represents the material time derivative (the cytosol is assumed to be moved with the cytoskeleton, convection of cytosol is not considered here), $\Delta = \frac{\partial^2}{\partial x^2} + \frac{\partial^2}{\partial y^2}$ is the Laplace operator, D_ξ and D_ζ are the protrusion and retraction diffusion constants in the membrane, K_0^ξ, K_M^ξ, and K_T^ξ are the rate constants for the spontaneous, auto-activation, and stress-mediated protrusion signal activations, K_0^ζ is the spontaneous activation rate for retraction signal, K_{off}^ξ and K_{off}^ζ are the decay constants for the protrusion and retraction signals, respectively. Here, ξ_0, ζ_0, n_1, n_2, n_3 are model parameters describing the auto-inhibition relation between the protrusion and retraction signals, R_ξ and R_ζ denote strength of random noise for protrusion and retraction signals, respectively, $G(t)$ is a Gaussian random process of mean zero and variance unity and $\langle G(t)\,G(t')\rangle = \delta(t-t')$, ξ_i and ζ_i are the volume concentration of the inactive forms of protrusion and retraction signaling molecules in the cytosol, which are in units of μm^{-3}. The diffusion of inactive protrusion and retraction signaling molecules in the cytosol are considered much faster than in the membrane. To be simple, ξ_i and ζ_i are assumed to be uniform in the cytosol and are calculated by the following two equations, respectively,

$$h_c\xi_i = h_c\xi_a - \bar{\xi} \tag{9}$$

$$h_c\zeta_i = h_c\zeta_a - \bar{\zeta} \tag{10}$$

where ξ_a and ζ_a are model parameters denoting the total volume concentrations of both active and inactive forms for protrusion and retraction signals, respectively, $\bar{\xi}$ and $\bar{\zeta}$ are the spatial mean values of ξ and ζ, respectively. In Eq. (9), multiplying ξ_i by cell thickness h_c to convert a volume concentration to an area concentration is based on the assumption that the cell is flat and the diffusion in the cell thickness direction is instantaneous.

2.3. Movement of the cell (i.e., protrusion and retraction)

The movement of the cell consists of the cell protrusion caused by the actin polymerization at the leading edge of the lamellipodia and the passive retraction as a result of active cytoskeleton contraction. A protrusion velocity $\boldsymbol{v}^p$ is defined as a function of the protrusion signal at the cell edge Γ as

$$v_i^p = c_p H(\xi - \xi_p)\,H(A_{\max} - A_c)\,\rho\xi\,n_i \tag{11}$$

where model parameter c_p represent the intrinsic level of membrane protrusion speed, parameter ξ_p is the threshold of protrusion signal above which membrane protrusion occurs, parameter $A_{\max}$ sets an upper limit of the cell area, n_i is the outward normal unit vector at the cell edge and index i takes values of 1 and 2 in 2D. The retraction velocity is assumed to be proportional to the instantaneous displacement u_i of the cytoskeleton as,

$$v_i^R = c_r u_i H(A_c - A_{\min}) \tag{12}$$

where c_r is a model parameter, $A_{\min}$ is the lower limit of the cell area.

2.4. Cytoskeletal asymmetry

Experimental studies have revealed that the cell polarity (i.e., head-and-tail pattern) is maintained through the long-lived cytoskeletal asymmetries including microtubules [33]. To incorporate the cytoskeletal asymmetries in the model, a vector $\boldsymbol{M}$ is defined to represent the polarity of the asymmetric cytoskeleton and its time evolution equation is defined as,

$$\frac{d\boldsymbol{M}}{dt} = K_M\left(\boldsymbol{M}_\xi - \boldsymbol{M}\right) \tag{13}$$

where K_M is a model parameter, $\boldsymbol{M}_\xi$ is a vector defined based on the protrusion signal,

$$\boldsymbol{M}_\xi = \frac{m_c}{A_c}\oint_\Gamma \xi\,|\boldsymbol{r}_e|^2\,\hat{\boldsymbol{r}}_e\,d\theta \tag{14}$$

Where m_c is a model parameter, $\hat{\boldsymbol{r}}_e = \boldsymbol{r}_e/|\boldsymbol{r}_e|$ is a unit vector and $\boldsymbol{r}_e$ is the position vector of the edge points relative to the center of the cell, $|\boldsymbol{r}_e|$ is the length of $\boldsymbol{r}_e$, $d\theta$ is the differential angle corresponding to the differential arc length, where θ is the angle coordinate of the edge point in the polar coordinate system

with the cell center as the origin. As implied by Eq. (13), in the steady-state ($d\boldsymbol{M}/dt = 0$), the cytoskeleton asymmetry vector $\boldsymbol{M}$ is equal to the vector $\boldsymbol{M}_\xi$. The cytoskeleton-asymmetry function $f_M(s)$ in Eq. (7) is defined with the polar angle θ_M of the vector $\boldsymbol{M}$ as,

$$f_M(\theta) = ((1 + cos(\theta - \theta_M))/2)^{n_M} \tag{15}$$

where n_M is a model parameter.

2.5. Cell–substrate interaction module

To incorporate the dynamic remodeling of focal adhesion, a phenomenological variable ρ is defined to describe the density distribution of focal adhesion-associated proteins (e.g., integrins, talins, vinculins, etc.). Variable ρ is normalized by the saturation value, thus ranges from zero (no integrin-mediated cell–substrate adhesion) to one (mature FAs). The time evolution of ρ is described by

$$\frac{D\rho}{\partial t} = \left[K_0^\rho + K_\xi^\rho \xi + K_T^\rho \left(\frac{T^{n_4}}{T^{n_4} + T_0^{n_4}}\right)\rho + K_M^\rho f_M \rho\right]\rho_i - K_{off}^\rho \rho + \sqrt{R_\rho} G(t), \tag{16}$$

where K_0^ρ, K_M^ρ, K_ξ^ρ, and K_T^ρ are the rate constants for the spontaneous, auto-activation, protrusion signal-dependent, and stress-mediated focal adhesion formation, respectively, K_{off}^ρ is a decay constant, T denotes the magnitude of the traction stress, T_0 and n_4 are model parameters, and R_ρ is the strength of random noise. Here the redistribution (e.g., via active transportation and passive diffusion) of unbound focal adhesion proteins is assumed to be faster than other time scale of focal adhesion formation, the unbound focal adhesion protein density ρ_i in the membrane is simply computed as

$$\rho_i = \rho_a - \bar{\rho} \tag{17}$$

where $\bar{\rho}$ is the mean value of ρ in the membrane domain, and ρ_a represents the average density of the total amount of bound and unbound focal adhesion proteins. Denoting k_{FA} and k_{ECM} the equivalent spring constants of the focal adhesion and the substrate, respectively, the spring constant of the cytoskeleton-substrate linkage is given as

$$k_{cs} = (k_{FA} k_{ECM})/(k_{FA} + k_{ECM}) \tag{18}$$

The mechanics of the cell is coupled to the dynamics of focal adhesion remodeling through the spring stiffness k_{FA} by the following relation

$$k_{FA} = k_{FA}^{max} \rho \tag{19}$$

where k_{FA}^{max} is the maximal stiffness when the focal adhesion density $\rho = 1\ \mu m^{-2}$ (i.e., mature focal adhesion).

2.6. Numerical implementation of the model

The cell monolayer model is implemented in an in-house code using the finite element method, where Lagrangian mesh is adopted and 3-node triangle element is used. The simplest Euler method for numerical integration is used for the time integration of the dynamic equations (e.g., Eqs. (5), (7), (8), etc.). Sufficiently small time step is used to ensure the stability and accuracy of the time integration. In the simulations of the movement of the cell, the mesh that represent the cell is moving with respect to the substrate. During each time step, the nodal spatial coordinates are updated as follows. The protrusion and retraction velocity of the Lagrangian mesh is calculated based on Eqs. (11) and (12). The displacement is then calculated and the new coordinates of the nodes of the mesh is updated. An auto mesh-generating algorithm based on Delaunay triangulation is utilized to perform re-meshing when mesh distortion occurs. Mesh transfer for the field variables is performed between the old and new meshes.

2.7. Integrating biomechanics and biochemistry in cell migration at the whole-cell scale

The coupling of different modules in our model are illustrated in Fig. 2. Starting from the middle left block, cell contraction generates mechanical stresses in the cell. These forces are converted into biochemical activities through mechanosensors, which in turn regulate the assembly/disassembly of macromolecular entities (upper and middle right blocks) and the cell protrusion/retraction (lower left block). The macromolecular assembly/disassembly alter the structural, geometrical, and material properties of the cell, which, according to the continuum/structural mechanics theory, will subsequently change both the internal stress (cytoskeleton stress) and stress at the boundary (i.e., cell–matrix adhesion stress). Thus, mechanics of the cell, biochemical activities, and macromolecular assemblies are coupled through mechanobiochemical feedback loops. Through such a mechanobiochemical system, the cell can sense the non-specific mechanical cues of its microenvironment. The crucial part of this system is the active contraction of the cell. Without the actomyosin contraction, no forces will be generated and cellular mechanosensors will not be activated.

3. Results and discussions

3.1. Comparison with the experimental data

To check whether the contraction submodel can capture the essential characteristics of the traction force distributions, traction-force microscopy experiments were conducted with MDA-MB-231 breast cancer cells cultured on the polydimethylsiloxane (PDMS) micro-post array substrate. For the micro-posts, the circular cross-section measures 0.8 μm in diameter, the height is 4.77 μm, and the spring stiffness is 1.389 nN/μm, which is equivalent to an elastic continuous media with Young's modulus of 2.44 kPa. The top of PDMS micro-posts were coated with collagen I by microcontact-printing and labeled with DiI, and the substrates were then soaked in pluronics F-127 to prevent cell adhesion to the side of micro-posts [34,35]. MDA-MB-231 cells were cultured on micro-post substrates overnight before the live-cell imaging. Fig. 3 (first two rows) shows the quantitative experimental data for the substrate displacement and traction force distribution during the cell migration process (see Video S1 and S2).

The cell shape in the experimental data at each time snapshots were extracted and used in the simulations as the input. In the simulations, the protrusion/retraction movement of the cell was turned off. The baseline contractility $\sigma_{c0} = 0.1$ kPa and the shear modulus of the cytoskeleton $G = 0.5$ kPa were used for the simulations, so that the predicted maximal magnitude of the traction force is close to the experimental data. As shown in Fig. 3 (3rd and 4th Rows), both the pattern of the predicted displacement and traction force distribution qualitatively match with the experimental results. The larger traction forces are localized to the two ends of the elongated cell.

Note that in one of the experimental images (indicated by the arrow), the high traction stress was not located at the tip of the cell, which is different than the corresponding model calculation. This discrepancy is interpreted as follows. The modeling results were from the steady state of the dynamic simulations, under the assumption that the time scale of cell shape change is much slower than other time scales in the dynamic model. The model also lacks the consideration of spatial and temporal heterogeneities in the cell. As a result, our present mathematical model will always predict higher traction stress at the outmost edge of the cell because of the principle of static equilibrium

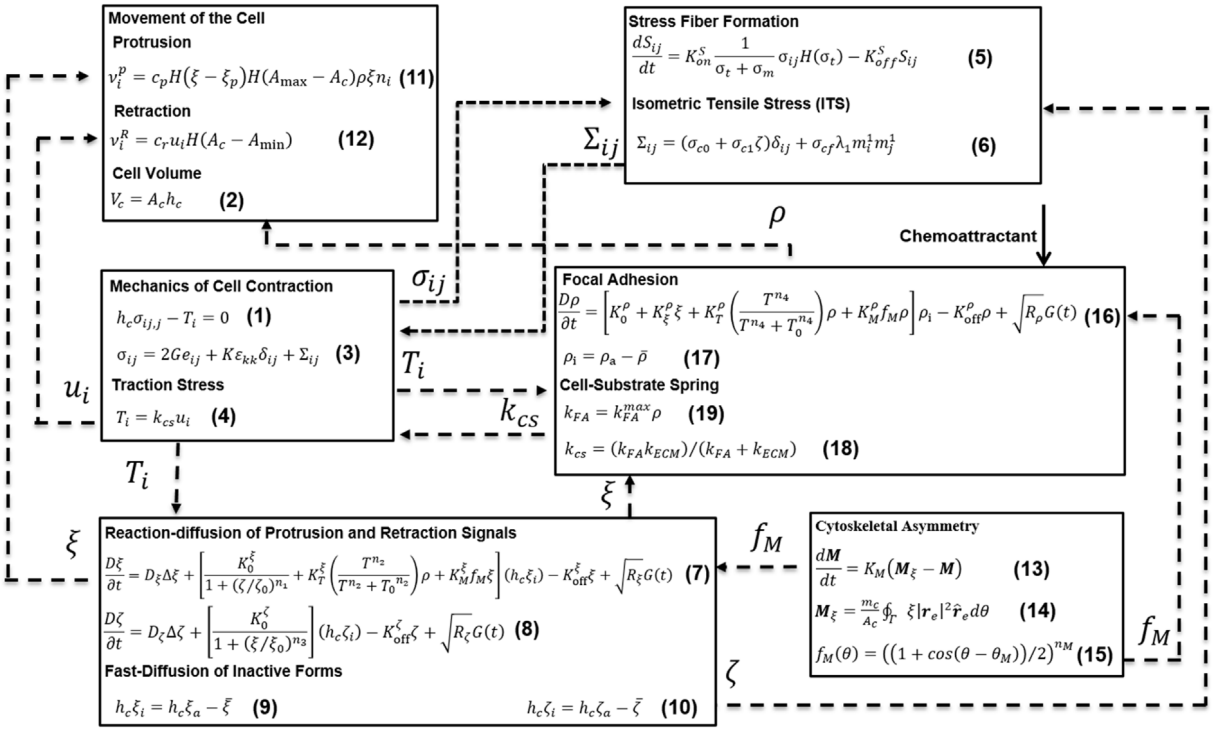

Fig. 2. Block diagram of the cross talks between the different modules of the cell model.

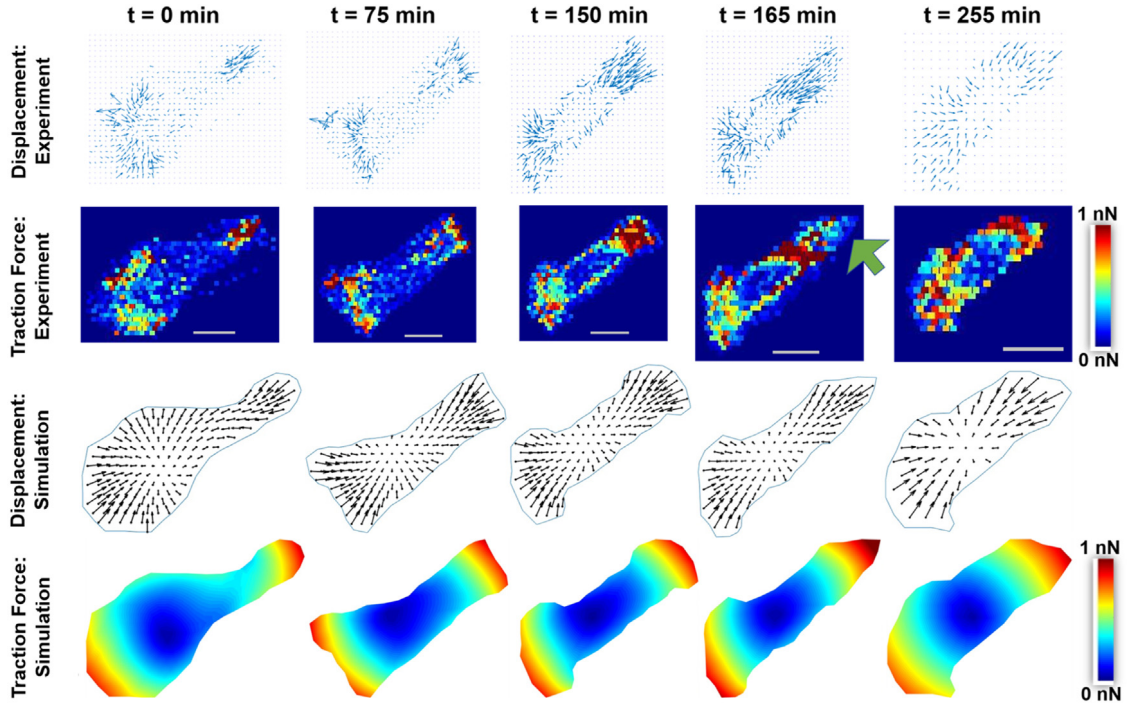

Fig. 3. Comparison of the traction force and displacement distribution between the experiment and the simulation of the contraction submodel. (See Video S1 and S2).

[29]. While in the experiment the cell is more transient and dynamic. For the cell at t=165 min time frame, the upper-right part marked by the arrow is the tail of the cell that was retracting. The retracting of the tail may have not completed, leaving a tail with weak adhesion and thus small traction stress.

3.2. Establishment of polarity of the cell with the reaction–diffusion submodel

Cell polarization (i.e., forming head and tail) is critical in cell migration to achieve directed movement. The spontaneous

polarization has been thought as a pattern formation in reaction–diffusion systems [12,32,36]. We here define the subsystem of equations consisting of Eqs. (7)–(10), where K_T^{ξ} and K_M^{ξ} are set to be zero, as the reaction–diffusion submodel. In this reaction–diffusion submodel, which were previously proposed by Maree et al. [13], the protrusion signal ξ and retraction signal ζ inhibit each other through the K_0^{ξ} and K_0^{ζ} terms, respectively. As studied by Maree et al. this simple mutual-inhibition model can induce spontaneous polarization. Fig. 4 shows the simulation result of the reaction–diffusion submodel. As shown in Fig. 4A (top row), starting with a randomly perturbed initial state, the protrusion signal ξ in a circular cell spontaneously polarizes, i.e., spatially separates into two zones: high and low regions. Because of the auto-inhibition, retraction signal distribution also polarizes (see Fig. 4A, second row).

As previously showed by Maree et al. [32], the cell shape (i.e., the shape of the mathematical domain of the reaction–diffusion equations) has an important effect on the spatial patterns formed. They concluded that at the steady state, the length of the interface that separates the high and low regions is minimized. Our simulation results agree with their conclusion. As shown in Fig. 4B, the interface in the elliptic cell is initially setup to be parallel to the longer axis of the ellipse (i.e., the initial distribution of the protrusion signal is a gradient from high in the left to low in the right). Over time, the interface rotates and eventually aligns with the shorter axis of the ellipse. To see how various model parameters, influence the steady-state protrusion and retraction distributions in the reaction–diffusion submodel, a rectangular (with an aspect ratio of 1:3) cell shape is used to simulate approximately a quasi-1D domain. The simulation results for parameter ζ_a, ζ_0, K_0^{ξ}, and K_{off}^{ξ} are plotted in Fig. 4C–F. One can see that change of these parameters can all shift the position of the interface and the peak value of ξ at the steady state.

3.3. Focal adhesion stress-dependent protrusion signal distribution

The reaction–diffusion submodel described above can account for the polarization of the protrusion signal, but it cannot explain the phenomenon observed in the previous study [23] in which the membrane protrusion localized to the four corners of the square cell. As shown in Fig. 5A, the reaction–diffusion submodel alone predicts a polarized pattern for the protrusion signal distribution in a square cell.

The previous studies showed that localization of the traction stress (which is equal to the focal adhesion stress) at the corners of the square cell is simply due to the mechanics principle of static equilibrium of an elastic body [28,37]. Based on that, we argue that protrusion signal and focal adhesion assembly can be enhanced by the mechanical stress in the focal adhesion. This hypothesis is implemented in our model by introducing the K_T^{ξ} term in Eq. (7) and the K_T^{ρ} term in Eq. (16).

We define the system of equations consisting of Eqs. (1)–(10) and Eqs. (16)–(19), where K_M^{ξ} and K_M^{ρ} are set to be zero, as the contraction–reaction–diffusion (CRD) model. Simulations results of the CRD model for the square shape are presented in Fig. 5B–C, showing the protrusion signal (Fig. 5B) and the localization of high traction stress (Fig. 5C), at the corners of the square cell. In a dynamic process, the localization to the corners is due a positive feedback loop in the CRD model: larger traction stress T leads to bigger ρ (Eq. (16)), larger ρ leads to bigger k_{cs} (Eqs. (18) and (19)), bigger k_{cs} results in larger traction stress T (Eq. (4)).

3.4. The role of the cytoskeleton asymmetry to the persistent migration

In this model, we introduce a cytoskeleton-asymmetry function $f_M(s)$ to be able to explicitly control the directional persistence of migration. Fig. 6 illustrates the role of function $f_M(s)$ in cell migration, in which the first two rows correspond to the simulation results of the protrusion signal and traction stress when the cytoskeleton asymmetry is turned off (i.e., setting $K_M^{\xi} = K_M^{\rho} = 0$), while the bottom two rows correspond to the simulation when the cytoskeleton asymmetry is on. Both simulations start with a circular cell and polarized protrusion signal (i.e., we initialize a spatial gradient for the distribution of the protrusion signal within the cell domain). When the cytoskeleton asymmetry is turned off (see the top two rows), the cell first becomes an elliptic shape due to the protrusion on the front of the cell and the retraction on the back of the cell. The interface line that divides the high and low protrusion signal regions is parallel to the longer axis of the ellipse. Then the cell front turns due to the turning of the interface line toward the shorter axis of the ellipse (see Video S7). On contrary, when the cytoskeleton asymmetry is turned on (bottom two rows), the cell shape becomes elongated in the dynamic equilibrium of the process of protrusion and retraction, and the cell preserves migration direction (see Video S8).

3.5. Simulation of durotaxis

Durotaxis is a term coined by Lo et al. [15], which refers to the substrate rigidity-guided cell migration. They showed in the *in vitro* experiment where a fibroblast cell crawls from the stiffer side of the substrate toward the softer side, the cell made a 90-degree turn at the interface to avoid migrating into the softer region. A conceptual two-step theory consisting of the force generation and mechanotransduction has been proposed previously by Lo et al. [15] to explain the durotaxis. A simple mechanics model has been presented by us previously to explain how exactly the larger focal adhesion stress is generated at the stiffer region of the substrate [29]. We showed that static equilibrium of the adherent cell along can yield the disparate traction stress on regions of different rigidity. In this study, we integrate the elasticity model with the reaction–diffusion equations to form a contraction–reaction–diffusion system. The dynamic model of single-cell migration is used to reproduce durotaxis phenomenon *in silico*.

As shown in Fig. 7, in the beginning of the simulations, the cell has a polarized circular shape and is placed on the stiffer region of the substrate (also see Video S9 and S10). During the simulations, the cell crawls toward the softer region (i.e., left side). The only difference between the two simulations (Fig. 7A and B) is the stress-dependent protrusion signal parameter K_T^{ξ}: relatively low for the simulation I (Fig. 7A) and high for the simulation II (Fig. 7B). Note that parameter K_T^{ξ} regulates the level of force-dependent activation of protrusion signal. At relatively low value of K_T^{ξ} (Fig. 7A), the cell crosses the interface with a slight change of cell shape (see Video S9). At a higher value of K_T^{ξ}, the cell makes a turn at the stiff-to-soft interface and then crawls along the interface (see Video S10). The turning of the cell at the interface is caused by the positive feedback loop mentioned previously in Fig. 5: larger substrate stiffness leads to larger traction stress and in turn leads to higher level of focal adhesion and protrusion signal, which results in change of migrating direction at the interface. These simulation results show that our model can successfully recapitulate durotaxis *in silico*.

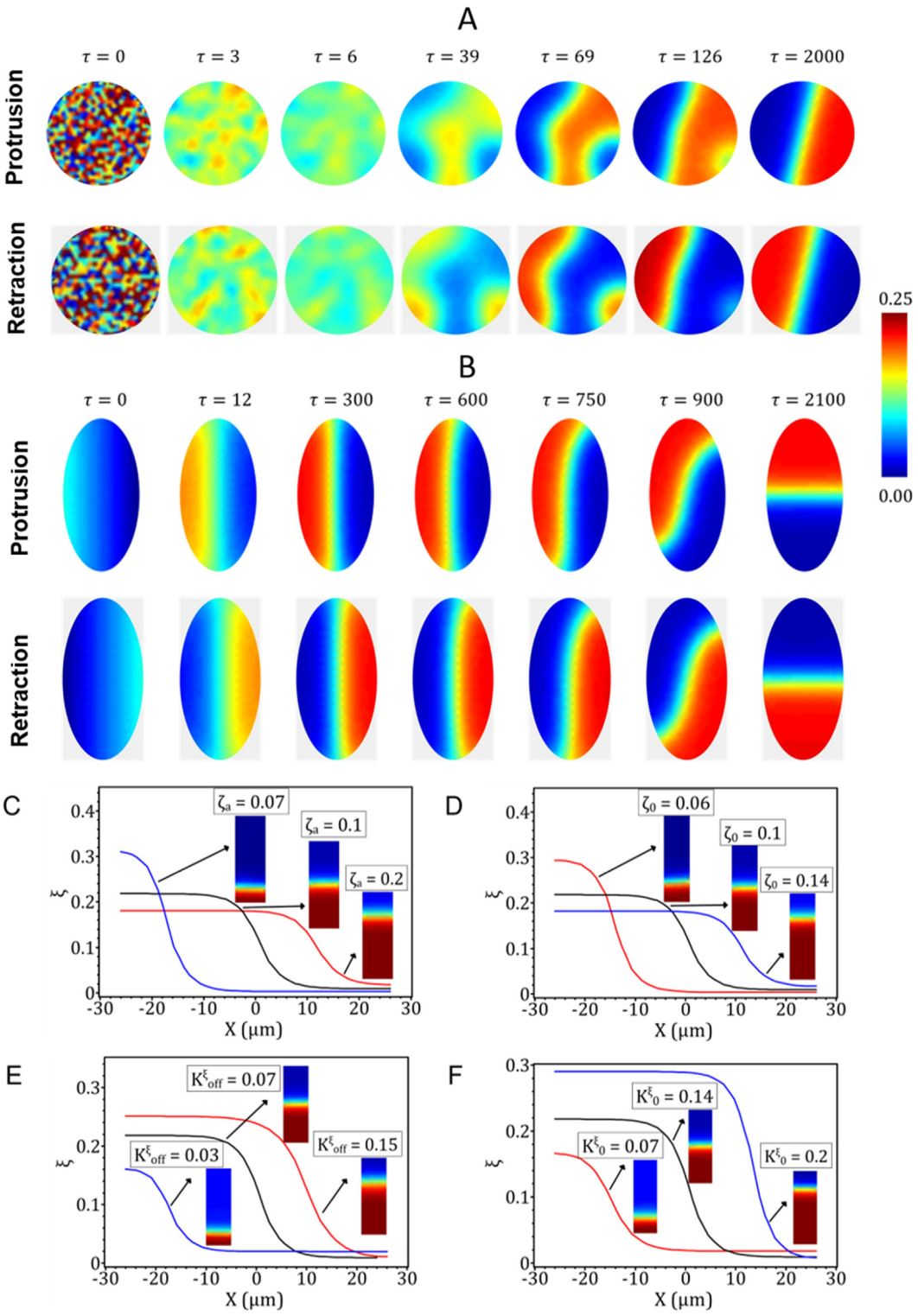

Fig. 4. Establishment of polarity of the cell with the reaction–diffusion submodel. (A) In a circular cell, protrusion signal ξ (and retraction signal ζ) polarizes spontaneously with random initial perturbation. (B) The effect of cell shape on the spatial patterns of protrusion signal ξ (and retraction signal ζ) in an elliptical cell. (C)–(F) Effect of modal parameters ζ_a, ζ_0, K_0^{ξ}, and K_{off}^{ξ} on the steady-state distribution of protrusion signal ξ. Note that all the panels share the same color bar. (See Video S3 and S4).

3.6. Cell shape as an emergent property

Cell shape is an emergent property of a cell during cell spreading and migration. Here the parameter space of the model was searched to identify the cells of different shapes. To quantitatively characterize the cell shape, we define two dimensionless numbers: the roundness and branchness numbers. The roundness number, denoted by Rn, was defined as $Rn = A/(\pi\tilde{r}^2)$ where A is the area of the cell, $\tilde{r}$ is the radius of the circle that circumscribe the cell boundary [12]. The roundness number Rn takes maximal value of 1 when the cell shape is a perfect circle and is smaller than 1 for any other shapes. The roundness number is useful

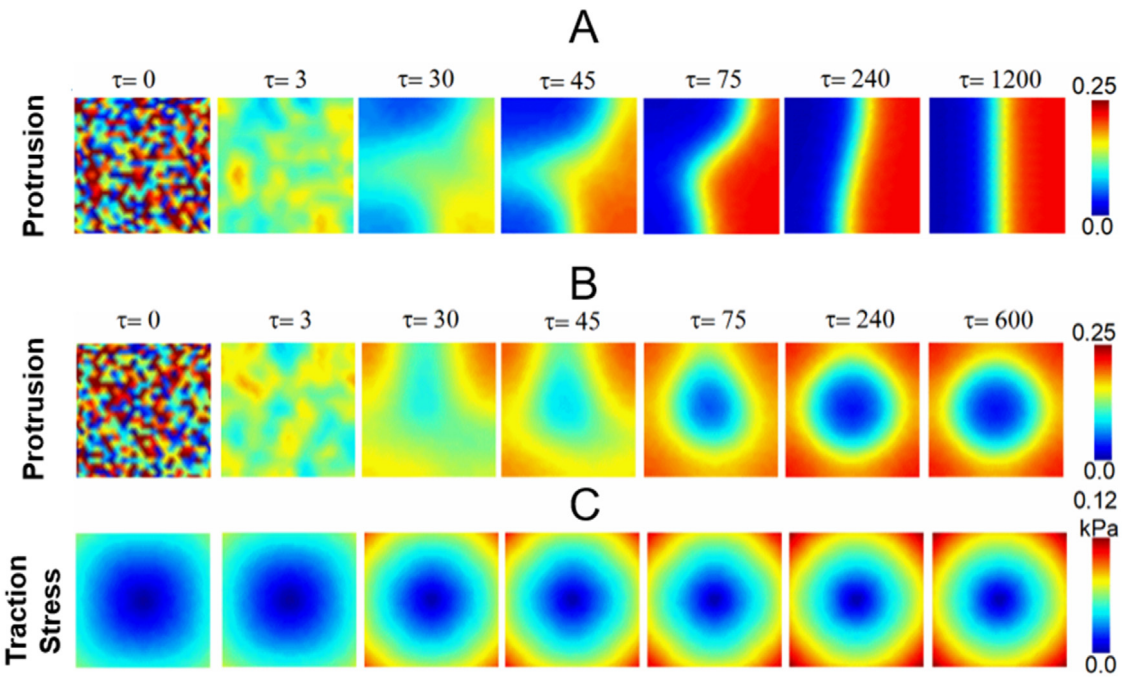

Fig. 5. The effect of mechanobiochemical coupling to the protrusion signal. (A) Protrusion signal ξ forms gradient pattern spontaneously with random initial perturbation. (B) Traction stress contour, with coupling protrusion signal. (C) Protrusion signal ξ forms circular pattern, with coupling traction stress, (i.e., turning on stress dependent activation parameter, $K_T^{\xi} = 0.45$) (See Video S5 and S6).

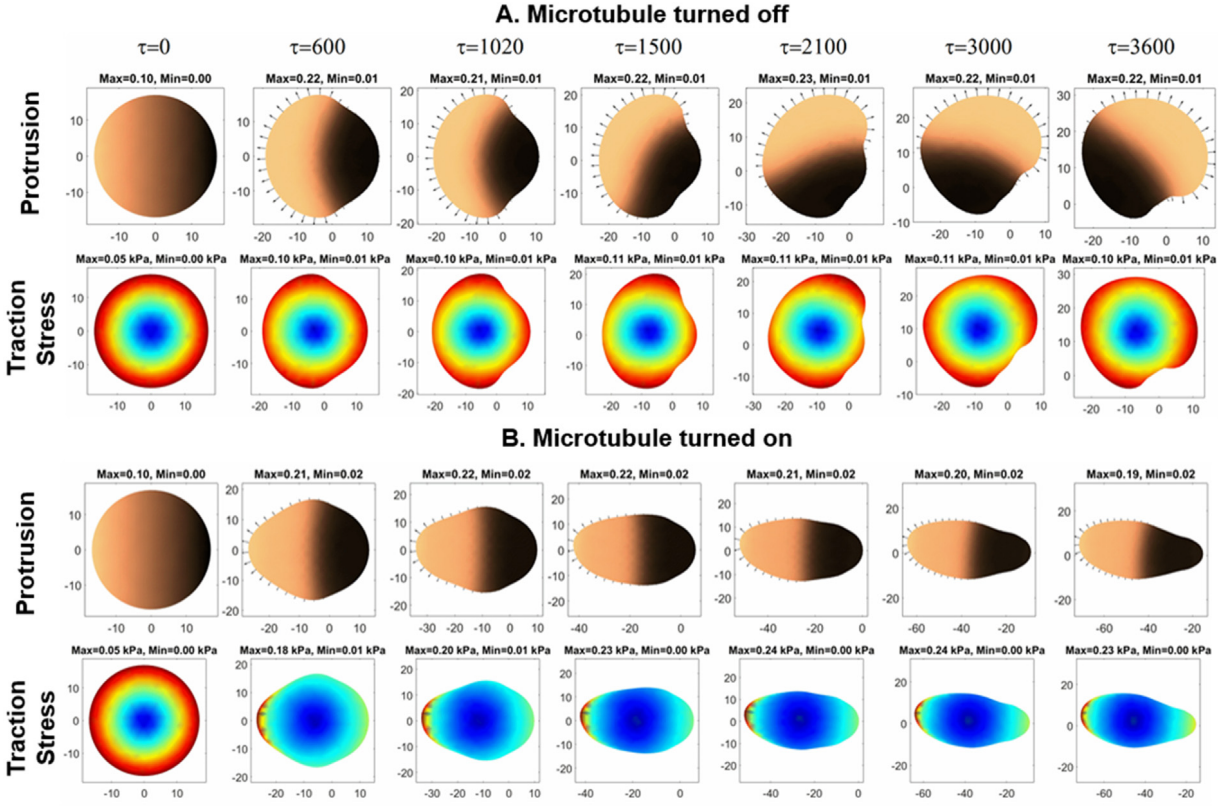

Fig. 6. The role of the cytoskeleton asymmetry to the persistent migration. The first and third rows: protrusion signal. The second and fourth rows: traction stress. For the first 2 row the Microtubule effect is simply turned off by setting the $K_M^{\rho} = 0$ and $K_M^{\xi} = 0$ For the third and fourth row, we just simply turned on the microtubule by setting $K_M^{\rho} = 0.1$ and $K_M^{\xi} = 0.05$. (See Video S7 and S8).

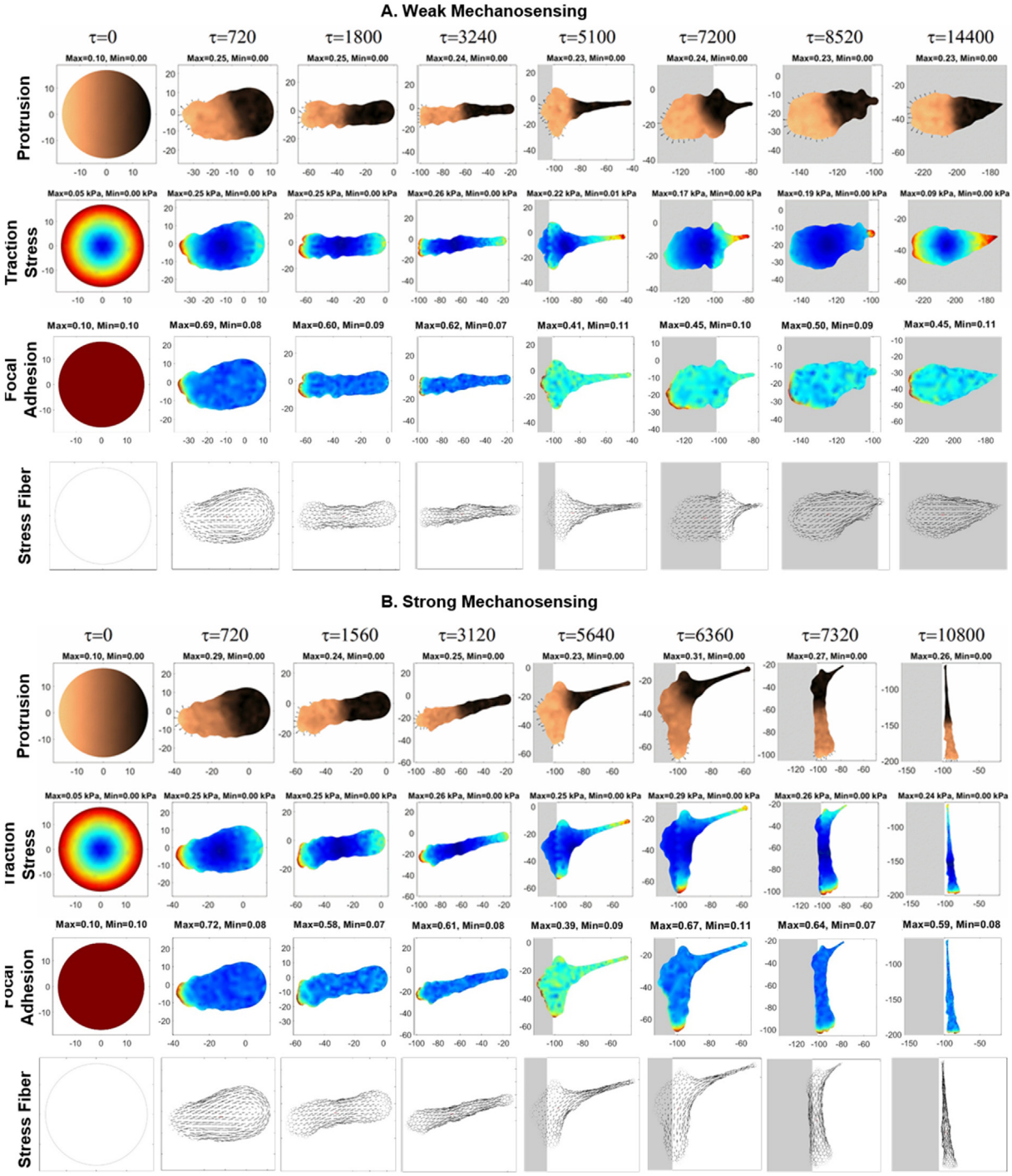

Fig. 7. Simulation of durotaxis (see Video S9 and S10) (A) At a smaller value of $K_T^{\xi} = 0.4$, the cell passes the interface. (B) At a larger value of $K_T^{\xi} = 0.6$, the cell turns at the interface. In both panel A and B, the first to fourth row plot the protrusion signal distribution, the traction stress, the focal adhesion, and the stress fiber orientation, respectively.

in distinguish between elongated and rounded shapes, but it fails to distinguish between the elongated and dendritic shapes. To identify the dendritic shapes, the branchness number Bn is defined as $Bn = \frac{L}{2\pi\bar{r}} - \frac{2}{\pi}$, where L is the perimeter of the cell. The branchness number Bn has a lower bound of zero when the cell shape approaches a strip with zero width and increases with increasing number of branches.

As shown in Table 1, two characteristic shapes: elongated (see Video S11) and dendritic (see Video S12), were identified in the parameter space search. The brute-force approach was used for the parametric study. The values of some of the key model parameters that corresponds to two characteristic shapes are listed. Note that the parameter values are given as the ranges within which these characteristic shapes occur. For the formation of elongated fibroblast-like shapes, as shown in the previous section, the cytoskeletal asymmetry is necessary for maintaining a non-rotating polarized shape. Therefore, parameters K_M^{ξ} and K_M^{ρ} both have a non-zero lower bound in order to form an elongated fibroblast-like cell. For the formation of dendritic shapes, larger values of ξ_p and c_p are required to create local pointwise protrusions. Interesting, the parameter study shows that large values

Table 1
Characteristic cell shape simulated by the cell model (see Video S11 and S12).

Parameters	Cell shape	
		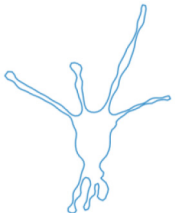
	Roundness = 0.47 **Branchness = 0.14**	**Roundness = 0.1** **Branchness = 0.79**
ξ_p (1 μm^{-2}) Protrusion threshold	**0.0–0.3**	**0.1–0.3**
c_p (μm^5 s^{-1}) Protrusion speed coefficient	**0.1–1.0**	**0.2–1.1**
c_r (s^{-1}) Retraction speed coefficient	**0.02–0.3**	**0.0–0.03**
K_M^{ξ} Microtubule dependence protrusion activation	**0.0–0.3**	**0.2–1.2**
K_T^{ξ} Traction dependence protrusion activation	**0.0–0.1**	**0.3–1.1**
K_T^{ρ} Traction dependence Focal adhesion activation	**0.0–0.4**	**0.3–1.7**
K_M^{ρ} Microtubule dependence focal adhesion activation	**0.1–0.3**	**0.0–1**

of parameter K_T^{ξ} is also required for the formation of dendritic shapes. This is interpreted as that strong positive feedback between the traction force and the protrusion signal generation at the tip of tube-like membrane protrusion is important for the formation of dendritic shapes.

4. Conclusions

In this work, we developed a computational model that integrates spatiotemporally the biomechanical and biochemical events involved in cell migration at the whole-cell scale. These events were treated as modules, between which cross-talks are defined. We have shown that the reaction–diffusion submodel can simulate cell polarization (head-to-tail formation), the contraction–reaction–diffusion model can simulate the localization of protrusion signal to the corners of the square cell, and the cytoskeleton-asymmetry module can simulate the persistent migration. Importantly, by coupling the mechanosensing with membrane protrusion signals, we demonstrated that this mechanobiochemical model can simulate substrate rigidity-guided cell migration (i.e., durotaxis). Finally, the full model, when applied to dynamics of cell migration, can simulate cell shape formation, i.e., cellular morphogenesis.

Our computational model incorporates the reaction–diffusion equations with continuum mechanics equations, thus enabling *in silico* studies of the coupling between the biochemistry and mechanobiology. The finite element method-based numerical implementation of the model makes the computational model accurate and efficient in simulating cells with irregular shapes. The modular approach of the development of this phenomenological model makes it easy to be extended to incorporate more biophysical principles. Recent experimental findings on cellular mechanobiology [38–40] increase the need of mathematical/computational models to interpret the experimental data. The computational model and the computer program developed here can be used to help test hypothesis and gain understandings of the complex system of living cells and tissues.

Declaration of competing interest

The authors declare that they have no known competing financial interests or personal relationships that could have appeared to influence the work reported in this paper.

Acknowledgments

H.Y. acknowledge funding support from the ASME Haythornthwaite Research Initiation Grant Award (USA) and the funding support from Southern University of Science and Technology, China (sustech. edu.cn). Y.S. acknowledge funding support from the National Science Foundation, USA (CMMI 1662835).

Appendix A. Supplementary data

Supplementary material related to this article can be found online at https://doi.org/10.1016/j.eml.2019.100566.

References

[1] G. Danuser, J. Allard, A. Mogilner, Mathematical modeling of eukaryotic cell migration: insights beyond experiments, Ann. Rev. Cell. Dev. Biol. 29 (2013) 501–528.
[2] P. Devreotes, A.R. Horwitz, Signaling networks that regulate cell migration, Cold Spring Harbin Perspect. Biol. 7 (2015) a005959.
[3] A.J. Ridley, M. a Schwartz, K. Burridge, R. a Firtel, M.H. Ginsberg, G. Borisy, J.T. Parsons, A.R. Horwitz, Cell migration: integrating signals from front to back, Science 302 (2003) 1704–1709.
[4] A. Mogilner, G. Oster, Cell motility driven by actin polymerization, Biophys. J. 71 (1996) 3030–3045.
[5] J. Kang, R.L. Steward, Y.T. Kim, R.S. Schwartz, P.R. LeDuc, K.M. Puskar, Response of an actin filament network model under cyclic stretching through a coarse grained Monte Carl approach, J. Theoret. Biol. 274 (2011) 109–119.
[6] S. Walcott, S.X. Sun, A mechanical model of actin stress fiber formation and substrate elasticity sensing in adherent cells, Proc. Natl. Acad. Sci. USA 107 (2010) 7757–7762.
[7] A.F.M. Marée, P. Hogeweg, A.F.M. Mare, How amoeboids self-organize into a fruiting body: Multicellular coordination in Dictyostelium discoideum, Proc. Natl. Acad. Sci. 98 (2001) 3879–3883.
[8] O.M. Matsiaka, C.J. Penington, R.E. Baker, M.J. Simpson, Discrete and continuum approximations for collective cell migration in a scratch assay with cell size dynamics, Bull. Math. Biol. 80 (2018) 738–757.
[9] L. Lin, X. Zeng, Numerical investigation of the role of intercellular interactions on collective epithelial cell migration, Biomech. Model. Mechanobiol. 17 (2018) 439–448.
[10] L. Lin, X. Wang, X. Zeng, Geometrical modeling of cell division and cell remodeling based on Voronoi tessellation method, C. - Comput. Model. Eng. Sci. 98 (2014) 203–220.
[11] V. Tarle, E. Gauquelin, S.R.K. Vedula, J. D'Alessandro, C.T. Lim, B. Ladoux, N.S. Gov, Modeling collective cell migration in geometric confinement, Phys. Biol. 14 (2017).

[12] J. Satulovsky, R. Lui, Y. Wang, Exploring the control circuit of cell migration by mathematical modeling, Biophys. J. 94 (2008) 3671–3683.
[13] A.F.M. Marée, A. Jilkine, A. Dawes, V.A. Grieneisen, L. Edelstein-Keshet, Polarization and movement of keratocytes: a multiscale modelling approach, Bull. Math. Biol. 68 (2006) 1169–1211.
[14] P.A. Iglesias, P.N. Devreotes, Biased excitable networks: How cells direct motion in response to gradients, Curr. Opin. Cell. Biol. 24 (2012) 245–253.
[15] C.M. Lo, H.B. Wang, M. Dembo, Y.-L. Wang, Cell movement is guided by the rigidity of the substrate, Biophys. J. 79 (2000) 144–152.
[16] J.H.C. Wang, E.S. Grood, T.S. agnitude, C.G. Determine, The strain magnitude and contact guidance determine orientation response of fibroblasts to cyclic substrate strains, Connect. Tissue Res. 41 (2000) 29–36.
[17] S. Li, P. Butler, Y. Wang, Y. Hu, D.C. Han, S. Usami, J.-L. Guan, S. Chien, The role of the dynamics of focal adhesion kinase in the mechanotaxis of endothelial cells, Proc. Natl. Acad. Sci. USA 99 (2002) 3546–3551.
[18] C.S. Chen, Mechanotransduction - a field pulling together?, J. Cell Sci. 121 (2008) 3285–3292.
[19] A. del Rio, R. Perez-jimenez, R. Liu, P. Roca-Cusachs, J.M. Fernandez, M.P. Sheetz, Stretching single talin rod molecules activates vinculin binding, Science (80-.) 323 (2009) 638–641.
[20] Y. Xiao, D. Hayman, S.S. Khalafvand, M.L. Lindsey, H.-C. Han, Artery buckling stimulates cell proliferation and NF-κB signaling, Am. J. Physiol. - Hear. Circ. Physiol. 307 (2014) H542–H551.
[21] Q. Wei, C. Huang, Y. Zhang, T. Zhao, P. Zhao, P. Butler, S. Zhang, Mechanotargeting: Mechanics-dependent cellular uptake of nanoparticles, Adv. Mater. 30 (2018) 1–7.
[22] Y. Sun, C.S. Chen, J. Fu, Forcing stem cells to behave: A biophysical perspective of the cellular microenvironment, Annu. Rev. Biophys. 41 (2012) 519–542.
[23] K.K. Parker, A.L. Brock, C. Brangwynne, R.J. Mannix, N. Wang, E. Ostuni, N.A. Geisse, J.C. Adams, G.M. Whitesides, D.E. Ingber, Directional control of lamellipodia extension by constraining cell shape and orienting cell tractional forces, Faseb J. 16 (2002) 1195–1204.
[24] D. Kong, B.H. Ji, L.H. Dai, Stability of adhesion clusters and cell reorientation under lateral cyclic tension, Biophys. J. 95 (2008) 4034–4044.
[25] M. Yao, W. Qiu, R. Liu, A.K. Efremov, P. Cong, R. Seddiki, M. Payre, C.T. Lim, B. Ladoux, R.-M. Mège, J. Yan, Force-dependent conformational switch of α-catenin controls vinculin binding, Nature Commun. 5 (2014).
[26] J. Howard, S.W. Grill, J.S. Bois, Turing's next steps: the mechanochemical basis of morphogenesis, Nat. Rev. Mol. Cell. Biol. 12 (2011) 392–398.
[27] P.R. LeDuc, W.C. Messner, J.P. Wikswo, How do control-based approaches enter into biology?, Ann. Rev. Biomed. Eng. 13 (2011) 369–396.
[28] H. Yuan, B. Marzban, K.K. Parker, Myofibrils in cardiomyocytes tend to assemble along the maximal principle stress directions, J. Biomech. Eng. (2017) 139.
[29] B. Marzban, X. Yi, H. Yuan, A minimal mechanics model for mechanosensing of substrate rigidity gradient in durotaxis, Biomech. Model. Mechanobiol. 17 (2018) 915–922.
[30] V.S. Deshpande, R.M. McMeeking, A.G. Evans, A bio-chemo-mechanical model for cell contractility, Proc. Natl. Acad. Sci. USA 103 (2006) 14015–14020.
[31] M. Graessl, J. Koch, A. Calderon, D. Kamps, S. Banerjee, T. Mazel, N. Schulze, J.K. Jungkurth, R. Patwardhan, D. Solouk, N. Hampe, B. Hoffmann, L. Dehmelt, P. Nalbant, An excitable Rho GTPase signaling network generates dynamic subcellular contraction patterns, J. Cell. Biol. 216 (2017) 4271–4285.
[32] A.F.M. Maree, V.A. Grieneisen, L. Edelstein-Keshet, How cells integrate complex stimuli: The effect of feedback from phosphoinositides and cell shape on cell polarization and motility, PLoS Comput. Biol. (2012) 8.
[33] H.V. Prentice-Mott, Y. Meroz, A. Carlson, M.A. Levine, M.W. Davidson, D. Irimia, G.T. Charras, L. Mahadevan, J.V. Shah, Directional memory arises from long-lived cytoskeletal asymmetries in polarized chemotactic cells, Proc. Natl. Acad. Sci. 113 (2016) 201513289.
[34] J. Fu, Y. Wang, M.T. Yang, R.A. Desai, X. Yu, Z. Liu, C.S. Chen, Mechanical regulation of cell function with geometrically modulated elastomeric substrates. (2011) 7.
[35] X. Xue, Y. Sun, A.M. Resto-irizarry, Y. Yuan, K. Meng, A. Yong, Mechanics-guided embryonic patterning of neuroectoderm tissue from human pluripotent stem cells. (2018).
[36] S.J. Altschuler, S.B. Angenent, Y. Wang, L.F. Wu, On the spontaneous emergence of cell polarity, Nature 454 (2008) 886–889.
[37] V.S. Deshpande, R.M. McMeeking, A.G. Evans, A model for the contractility of the cytoskeleton including the effects of stress-fibre formation and dissociation, Proc. R. Soc. A 463 (2007) 787–815.
[38] C. Huang, T. Ozdemir, L.-C. Xu, P.J. Butler, C.A. Siedlecki, J.L. Brown, S. Zhang, The role of substrate topography on the cellular uptake of nanoparticles, J. Biomed. Mater. Res. B 104 (3) (2016) 488–495, http://dx.doi.org/10.1002/jbm.b.33397.
[39] Y. Zhang, X. Shi, T. Zhao, C. Huang, Q. Wei, X. … Tang, S. Zhang, A traction force threshold signifies metastatic phenotypic change in multicellular epithelia, Soft Matter (2019) http://dx.doi.org/10.1039/C9SM00733D.
[40] Y. Zhang, Q. Wei, T. Zhao, P. Zhao, S. Zhang, Extracellular and intercellular force distribution in circularly shaped epithelia, Extremes Mech. Lett. (2019) 100526, http://dx.doi.org/10.1016/j.eml.2019.100526.